THE JOURNAL OF PHYSICAL CHEMISTRY C

Article

pubs.acs.org/JPCC

Supercritical CO_2-Assisted Electrochemical Deposition of ZnO Mesocrystals for Practical Photoelectrochemical Applications

Wei-Hao Lin,[†] Tso-Fu Mark Chang,[‡] Yi-Hsuan Lu,[†] Tatsuo Sato,[‡] Masato Sone,[‡] Kung-Hwa Wei,[†] and Yung-Jung Hsu*[,†]

[†]Department of Materials Science and Engineering, National Chiao Tung University, Hsinchu, Taiwan 30010, Republic of China

[‡]Precision and Intelligence Laboratory, Tokyo Institute of Technology, 4259-R2-35 Nagatsuta-cho, Midori-ku, Yokohama 226-8503, Japan

ABSTRACT: We have successfully developed an effective supercritical CO_2 (sc-CO_2) emulsion-assisted electrochemical approach for cathodic deposition of ZnO mesocrystals. The sc-CO_2 was introduced along with a nonionic surfactant in the process to form emulsified electrolyte, which significantly increased the supersaturation degree and promoted the molecular diffusion to affect the crystal growth of ZnO. The deposition involved the generation of primary nanocrystals with substantially high surface energy, followed by the preferred attachment of the primary nanocrystals along an energetically favorable orientation to form ZnO mesocrystals. The as-deposited ZnO mesocrystals exhibited remarkable optical properties at room temperature in terms of prominent near band-edge emission and substantially long exciton lifetime, attributable to the highly oriented crystallinity of mesocrystals that effectively suppressed the nonradiative charge recombination to extend the exciton decay dynamics. As compared to the structures prepared without the addition of surfactant or sc-CO_2, ZnO mesocrystals from sc-CO_2 emulsion displayed greatly improved photoactivity toward photoelectrochemical water oxidation, revealing their promising potential as photoanodes in relevant photoelectrochemical processes. The current study delivers the first demonstration of directly depositing ZnO mesocrystals on conductive substrates, which paves the way for utilization of mesocrystals as practical electrodes in technologically important energy conversion fields, such as electrochemical cells, photovoltaic devices, as well as photoelectrochemical water splitting, where the advantageous structural characteristics of mesocrystals, i.e., high crystallinity and abundant porosity, can be fully exploited.

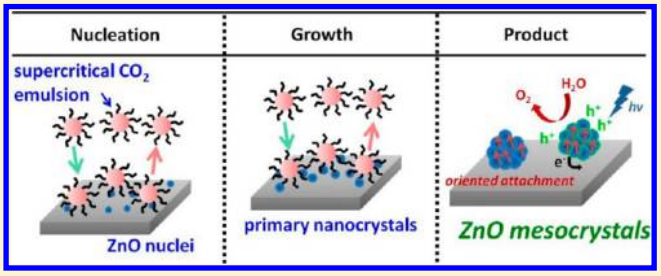

INTRODUCTION

As a new class of alternative crystals, mesocrystals have received considerable attention owing to their unique mesoscopic structures that may enable new materials applications.[1−3] These nonclassical crystals are highly ordered superstructures composed of nanocrystal building blocks assembled in a crystallographically oriented manner, which gives rise to mesoporous, single-crystal-like structural characteristics. The highly oriented crystallinity and abundant interior porosity make mesocrystals especially promising in applications requiring facile charge transport and high surface area, for example, catalysis, sensing, electrochemical energy conversion, and storage, as well as solar energy conversion.[4] Until now, a wide variety of mesocrystals including inorganic salts,[5,6] organic molecules,[7,8] metals,[9,10] and metal oxides[11−14] have been successfully prepared and explored to foster their practical utilizations.

In the past few decades, ZnO has stimulated great research interest due to its extensive applications ranging from photoelectronic physics to material chemistry.[15,16] Recent efforts have focused on the fabrication of ZnO with complex structural diversities of size, shape, and orientation to acquire the tailored properties.[17−29] With the wurtzite crystal structure constructed by alternating polar planes of (0001) and (000-1), ZnO possesses an intrinsic dipole moment along the *c*-axis direction, which can drive the assembly of the primary nanocrystals to form hierarchical mesocrystals.[17] On the other hand, by employing organic additives to manipulate the relative surface energy, organization of building units of ZnO can also be directed to produce ordered superstructures with minimized total surface energy.[18] There have been diverse synthetic methods developed to obtain hierarchical superstructures of ZnO, which include high-temperature vapor deposition,[19,20] polymer-mediated chemical reaction,[21−23] a two-step hydrothermal-annealing process,[24,25] and other facile one-pot solution-based methods.[26−29] These developments have witnessed a rising demand for sophisticated assembly of nanocrystal building blocks to achieve superior functionalities.

Among the different synthetic approaches, electrochemical cathodic deposition affords a simple yet effective process for production of ZnO with controllable morphology. Moreover, cathodic deposition enables direct deposition of ZnO structures

Received: September 26, 2013
Revised: October 24, 2013
Published: November 15, 2013

on conductive substrates, which may facilitate their utilization as practical electrodes in relevant electrochemical and photoelectrochemical processes. However, the adsorption of H_2 bubbles on the cathode surface[30] and the high surface tension of aqueous electrolyte[31] may cause structural defects in the deposited crystals. By introducing supercritical carbon dioxide (denoted as sc-CO_2) which shows high solubility toward H_2 and nearly zero surface tension in the cathodic deposition process, significantly improved crystallinity can be acquired for the product.[32,33] Besides, the use of sc-CO_2 is a clean and favorable approach for electrodeposition because of its intriguing attributes like nontoxicity, inexpensiveness, low viscosity, and high diffusivity. In this work, we developed an effective sc-CO_2 emulsion-assisted electrochemical process for cathodic deposition of ZnO mesocrystals on conductive substrates. The sc-CO_2 was introduced along with a nonionic surfactant in the process to form emulsified electrolyte. The deposition involved the generation of primary nanocrystals with substantially high surface energy, followed by the preferred attachment of the primary nanocrystals along an energetically favorable orientation to form ZnO mesocrystals. The as-deposited ZnO mesocrystals showed a prominent band-edge emission peak at 380 nm with a substantially long exciton lifetime of 10.2 ns, attributable to the highly oriented crystallinity of mesocrystals that effectively suppressed the nonradiative charge recombination to extend the exciton decay dynamics. As compared to the structures prepared by convectional depositions, ZnO mesocrystals from sc-CO_2 emulsion achieved significantly enhanced photocurrents of water oxidation, revealing their promising potential as photoanodes in relevant photoelectrochemical processes.

EXPERIMENTAL SECTION

Chemicals. All chemicals including CO_2 (Nippon Tansan Gas, 99.9%), polyoxyethylene lauryl ether ($C_{12}H_{25}(OCH_2CH_2)_{15}OH$, Toshin Yuka Kogyo, 25%), $ZnCl_2$ (Sigma-Aldrich, 98.0%), $NaNO_3$ (Sigma-Aldrich, 99.0%), H_2O_2 (Sigma-Aldrich, 30%), and NaCl (Sigma-Aldrich, 99.0%) were used as received without further purification.

Electrochemical Cathodic Deposition. The cathodic deposition of ZnO was conducted in a high-pressure, two-compartment cell,[32] which consisted of Al substrate (1.0 cm × 2.0 cm) as the working electrode and Pt foil (1.0 cm × 2.0 cm) as the counter electrode. The electrolyte comprised a mixed aqueous solution of 4 mM $ZnCl_2$, 80 mM NaCl, 56 mM H_2O_2, and 42 mM $NaNO_3$. For the deposition of ZnO mesocrystals, 0.16 vol. % surfactant and 20 vol. % CO_2 of 15 MPa were introduced in the electrolyte. Here the nonionic surfactant of polyoxyethylene lauryl ether was used to form the sc-CO_2-in-water emulsion in the electrolyte. The deposition was run with a constant current density of 0.15 A/dm^2 at 70 °C for 60 min. To unravel the role of sc-CO_2 emulsion in the formation of ZnO mesocrystals, conventional deposition without the addition of surfactant or sc-CO_2 and deposition with 0.16 vol % surfactant added were also performed. The as-deposited samples were washed with deionized water and then annealed at 400 °C for 30 min to remove the remaining surfactant.

Characterizations. The morphology and dimensions of the products were examined with a field emission scanning electron microscope (FESEM, Hitachi, S-4300SE). The crystallographic structure of the samples was investigated with X-ray diffraction (XRD, Rigaku, Ultima IV), transmission electron microscopy (TEM, JEOL, JEM-2100), and selected-area electron diffraction (SAED, an accessory of JEM-2100). For steady-state photoluminescence (PL) spectroscopy, a Kimmon IK3001R-G equipped with a He−Cd laser (720 W) was used. Time-resolved PL spectra were measured at room temperature using a single photon counting system (Horiba Jobin Yvon) which delivers an instrument response function down to 25 ps fwhm. The GaN diode laser (λ = 375 nm) was used as the excitation source. The signals collected at the PL emission peak of ZnO were dispersed with a grating spectrometer, detected by a high-speed photomultiplier tube, and then correlated using a single-photon counting card. The recorded emission decay data were analyzed and fitted with a biexponential kinetics model which generates two lifetime values, τ_1 and τ_2, and the corresponding amplitudes, A_1 and A_2. The intensity-average lifetime, $\langle\tau\rangle$, was then determined using the following expression $\langle\tau\rangle = (A_1\tau_1^2 + A_2\tau_2^2)/(A_1\tau_1 + A_2\tau_2)$. All the fitting results were summarized in Table 1. The near-unity value of goodness (χ^2) of the fitting implied a good fit to the experimental data. The photoelectrochemical measurement was conducted in a three-electrode cell which consisted of a Pt counter electrode, Ag/AgCl reference electrode, and 0.5 M Na_2SO_4 electrolyte. The as-deposited ZnO structures on Al substrate were used as a working electrode within the photoelectrochemical cell, and the chronoamperometric $I-t$ curves were recorded at 0 V vs Ag/AgCl under white light illumination (500 W xenon lamp, with a light intensity of 100 mW/cm^2).

Table 1. Kinetic Analysis of Emission Decay for ZnO Structures Prepared with Different Depsoition Conditions

	A_1 (%)	τ_1 (ns)	A_2 (%)	τ_2 (ns)	$\langle\tau\rangle$ (ns)	χ^2
conventional deposition	50.3	12.8	49.7	4.2	8.6	1.049
deposition with surfactant	49.5	11.7	50.5	3.7	7.3	1.160
deposition with sc-CO_2	64.2	13.3	35.8	4.7	10.2	1.075

RESULTS AND DISCUSSION

For cathodic deposition of ZnO which uses $ZnCl_2$, H_2O_2, and $NaNO_3$ as the electrolyte composition (the current pH value was 5.7), the reaction mechanism can be described by the following pathways[34−38]

$$NO_3^- + H_2O + 2e^- \rightarrow NO_2^- + 2OH^- \quad (1)$$

$$H_2O_2 + 2e^- \rightarrow 2OH^- \quad (2)$$

$$Zn^{2+} + 2OH^- \rightarrow ZnO + H_2O \quad (3)$$

Briefly, reduction of NO_3^- and H_2O_2 takes place to generate OH^- ions at the surface of the cathode (1, 2). The Zn^{2+} ions in the vicinity of the cathode then react with OH^- ions to form ZnO through proper dehydration (3). In addition to the primary pathways, reactions associated with gas evolution can also occur, which include H_2 production from H^+ reduction and generation of N_2 and NH_3 from additional NO_3^- reduction.[35] It has been reported that by suitably modulating the experimental conditions such as the precursor concentration, the deposition temperature, and the applied current density, the morphology of the grown ZnO in cathodic deposition process can be readily controlled.[36−38] Unlike most studies concerning electrochemical deposition of ZnO which explored the above-mentioned effects, the current study focuses on studying the influence of sc-CO_2 emulsion introduction on the crystal

dx.doi.org/10.1021/jp409607m | J. Phys. Chem. C 2013, 117, 25596−25603

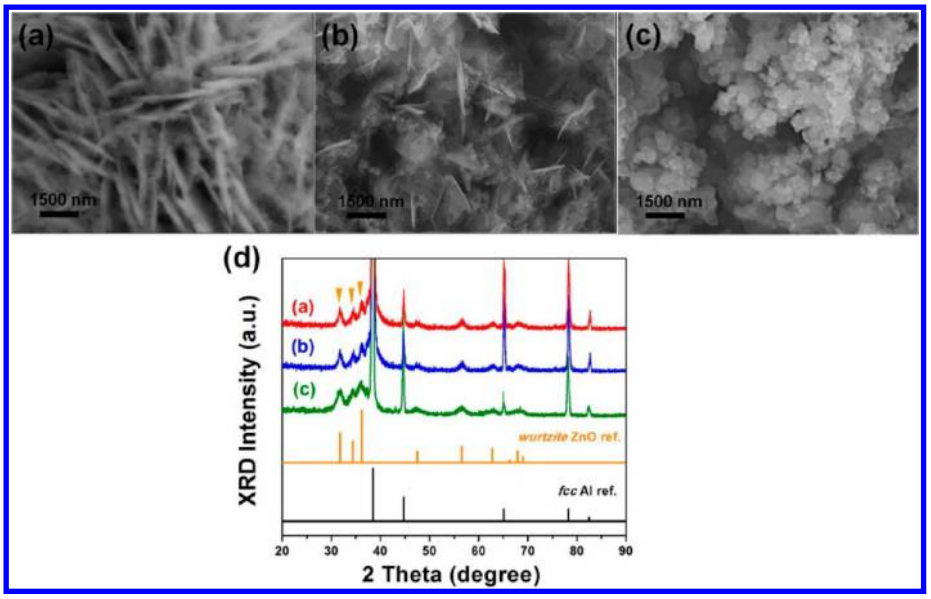

Figure 1. SEM images of ZnO structures prepared by (a) conventional deposition, (b) deposition with 0.16 vol. % surfactant, and (c) deposition with sc-CO_2 emulsified electrolyte. The corresponding XRD diffractograms were shown in (d), with the three characteristic peaks of wurtzite ZnO marked by arrows.

growth of the deposited ZnO. Figure 1 shows the SEM images and XRD diffractograms of the three ZnO samples prepared in this work. First, conventional cathodic deposition produced platelet-like structures on the substrate surface. As Figure 1(a) shows, these platelets had a typical thickness of 50−100 nm and an edge length up to several micrometers. With the addition of 0.16 vol. % surfactant in the electrolyte, platelet structures accompanied by appreciable amounts of nanoparticles were observed in the product, as evident from Figure 1(b). This phenomenon indicates that the added surfactant may have affected the growth of ZnO in the cathodic deposition process. When sc-CO_2 emulsified electrolyte was used, the grown ZnO was however characterized by particulate structures with relatively large dimensions. As Figure 1(c) shows, these particles had an apparent size of 200−400 nm, and if examined closely they were aggregates of tiny nanocrystals with sizes of 10−20 nm. The corresponding XRD diffractograms of Figure 1(d) confirm the composition of the three samples as pure wurtzite ZnO. It was noticed that the sample from sc-CO_2 emulsion exhibited broadened diffraction peaks of ZnO relative to the samples from the other two processes, which is in conformity with the considerably tiny size of the composing nanocrystals. Most importantly, the distinctive structural feature of particle aggregates for the sample obtained with sc-CO_2 emulsified electrolyte discloses the significant influence of sc-CO_2 emulsion introduction on the cathodic deposition of ZnO, as will be discussed later.

Further structural investigations on the as-deposited ZnO, especially the platelet structures from conventional deposition and the particle aggregates from sc-CO_2 emulsion, were carried out using TEM and SAED. As shown in Figure 2(a), the platelet structures from conventional deposition appeared to possess abundant voids on the surface. These defective voids might arise from the gas evolution issue in the typical cathodic deposition process.[32,33] The inset SAED shows a ring pattern of wurtzite ZnO crystal, suggesting that the platelet structures were polycrystalline. In Figure 2(b), the lattice-resolved TEM image clearly displays the (10-10) lattice plane of wurtzite ZnO

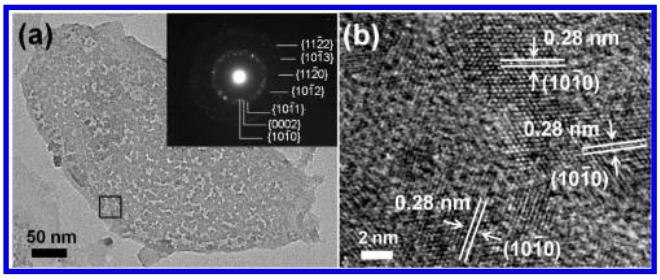

Figure 2. (a) Typical TEM and (b) HRTEM images of ZnO platelet structures prepared by conventional depostion. Inset in (a) shows the corresponding SAED pattern.

with a *d*-spacing of 0.28 nm. Besides, structural defects such as grain boundaries and disordered grain orientation were ubiquitously observed, which may account for the polycrystalline nature of the sample. For the particle aggregates obtained with sc-CO_2 emulsified electrolyte, they were constructed by mesoscale substructure instead of the atomic-level continuous structure, as revealed in Figure 3(a). The corresponding SAED shows a single-crystal-like dot pattern, implying that the composing nanocrystals were highly oriented and aligned. To verify such a crystallographic orientation feature, the detailed microstructures of the particle aggregates were investigated with high-resolution TEM (HRTEM). As illustrated in Figures 3(b)−(f), lattice fringes of (10-10) were found parallel throughout the whole particle aggregate. This outcome manifests that the primary nanocrystals of particle aggregates were well aligned in a common crystallographic fashion, which is a typical situation in mesocrystal assembly.[1−3] Furthermore, apparent interstices that have usually been regarded as mesopores in mesocrystal construction[17,39] were noticed at the boundaries between the primary nanocrystals. The HRTEM investigation together with the finding from SAED confirms that the particle aggregates prepared with sc-CO_2 emulsified electrolyte were ZnO mesocrystals.

Evidently, the introduction of sc-CO_2 emulsion resulted in the assembly of the primary nanocrystals in a crystallographic

dx.doi.org/10.1021/jp409607m | J. Phys. Chem. C 2013, 117, 25596−25603

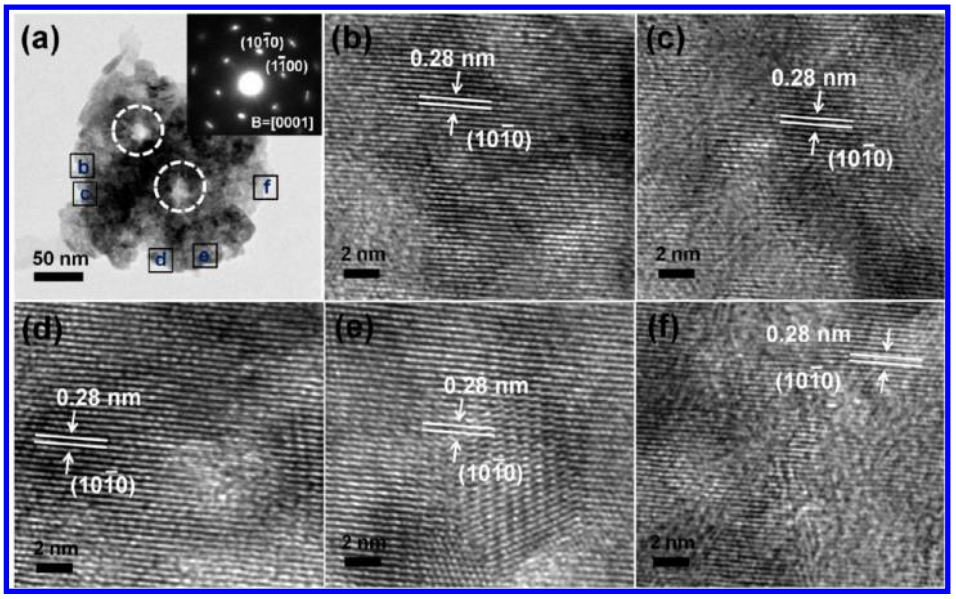

Figure 3. (a) Typical TEM image of ZnO mesocrystals prepared by deposition with sc-CO_2 emulsified electrolyte. The white circles represent the mesopores, and the inset shows the corresponding SAED pattern. (b)−(f) HRTEM images taken at the marked regions of (a).

Scheme 1. Schematic Illustration of the Growth Mechanism for ZnO Structures Prepared with Different Deposition Conditions

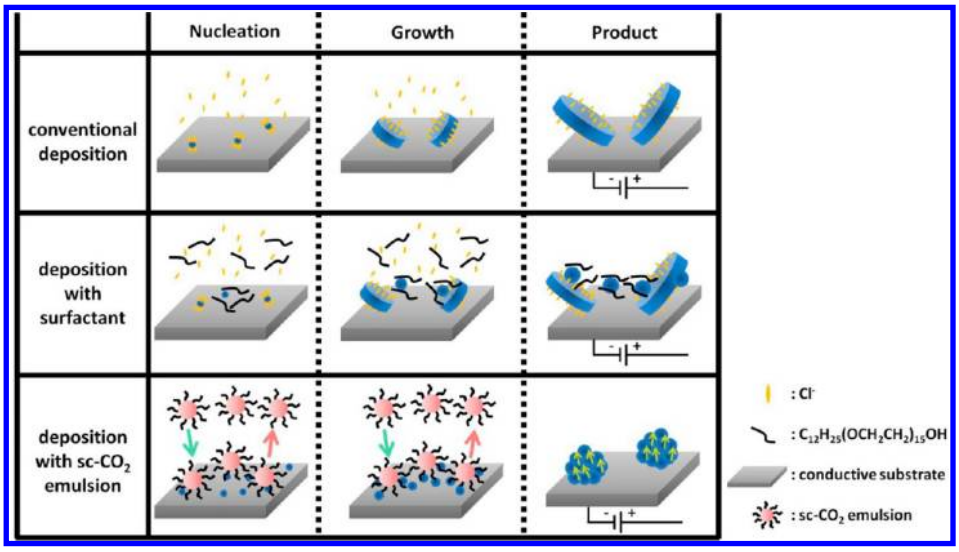

oriented manner to form the final mesocrystals. This delicate organization process is termed "oriented attachment" and has been widely documented in the literature regarding the formation of mesocrystals.[1−3] The so-called oriented attachment describes a spontaneous self-assembly process for adjacent crystals sharing a common crystallographic orientation, which leads to the formation of mesocrystals exhibiting mesoporous, single-crystal-like structural characteristics. In the present system, sc-CO_2 emulsion played a crucial role in facilitating the self-assembly of the primary nanocryatals to form ZnO mesocrystals. A plausible growth mechanism is proposed as follows. For conventional deposition, platelet structures were grown as a result of the selective adsorption of Cl^- ions on the (0001) facets of ZnO.[40] Such Cl^- adsorption could effectively retard the growth of ZnO along its [0001] direction, promoting crystal growth along the lateral directions of {10-10} to form two-dimensional platelet structures. The predominant lattice orientation of [10-10] observed in Figure 2(b) was consistent with this argument. The two-dimensional anisotropic growth of ZnO was to some extent disturbed when the nonionic surfactant of polyoxyethylene lauryl ether was added. Note that the pH value of the electrolyte containing 0.16 vol. % surfactant was 5.8, essentially lower than the isoelectric point of 9.5 of ZnO.[41] Under this circumstance, ZnO possessed positive surface charges which rendered the electrostatic interaction with surfactant molecules through binding to their negative charged ether groups.[42] The surfactant binding may compete with Cl^- adsorption on the ZnO surface to hinder the two-dimensional anisotropic crystal growth, thereby generating appreciable amounts of nanoparticles as observed. As sc-CO_2 emulsion was introduced, the pH value of the electrolyte decreased largely due to the partial dissolution of CO_2. Since the solubility of ZnO in water decreased with the fall of pH value,[43,44] a significant increase in supersaturation degree was considered for sc-CO_2 emulsified electrolyte. It has been reported that the supersaturation degree of the growing species plays a key role in determining the morphology of the grown crystals.[45] In general, a relatively low supersaturation is

dx.doi.org/10.1021/jp409607m | J. Phys. Chem. C 2013, 117, 25596−25603

required for anisotropic crystal growth to take place, above which isotropic growth happens. We surmised that the virtually high supersaturation degree of ZnO in sc-CO_2 emulsified electrolyte would trigger the isotropic growth regime for ZnO to generate isotropically shaped nanocrystals. The thus-generated ZnO nanocrystals should have possessed substantially high surface energy owing to the high supersaturation degree initially created.[46] On the other hand, the introduced sc-CO_2 emulsion can improve the diffusion efficiency for NO^{3-} and H_2O_2,[31] which enabled abundant OH^- generation to accelerate the nucleation and growth of ZnO. This may further expedite the isotropic crystal growth for ZnO to grow nanocrystals with considerably high surface energy. To reduce the total surface energy, the grown ZnO nanocrystals underwent preferred attachment along an energetically favorable orientation, eventually leading to the formation of ZnO mesocrystals. The parallel orientation of [10-10] throughout the whole particle aggregate as well as the nearly single crystalline SAED pattern supported the above contention. It should be noted that the electric field applied at the cathode might assist in directing the organization of the primary nanocrystals by interacting with the intrinsic fields of ZnO.[17] This interaction would spatially confine the oriented attachment to the cathode surface and result in the deposition of ZnO mesocrystals directly on the substrate. To summarize the proposed mechanism, a scheme is shown in Scheme 1 to illustrate the role of sc-CO_2 emulsion in the formation of ZnO mesocrystals from the present cathodic deposition process.

The present ZnO mesocrystals provided a versatile platform for the investigation of a mesoscopic structural effect on the intrinsic material properties of mesocrystals. We first used steady-state PL spectroscopy to examine the optical properties of the as-deposited samples. As displayed in Figure 4(a), all three ZnO structures exhibited pronounced PL emission in the wavelength range of 350−700 nm. For the platelet structures from conventional deposition, an emission band centered at 392 nm was observed, which is ascribed to the superposition of near band-edge UV emission and defect-related blue emission of ZnO.[47] For the platelet/particle composite structures from deposition with surfactant, a wide emission band spanning from the UV to visible region was recorded. This band, centered around 426 nm, was significantly broadened and red-shifted in comparison to the emission band of the platelet structures. This phenomenon suggests that the platelet/particle structures were characteristic of abundant structural defects and had multiple trap-state emissions[48] that were spectrally overlapped. As for the mesocrystals from sc-CO_2 emulsion, a prominent emission peak attributable to the excitonic band-edge emission of ZnO was measured at 380 nm. In addition, the trap-state emission band which can be identified beyond 450 nm was considerably weak, suggesting the inherently high crystallinity for ZnO mesocrystals as is consistent with the results from HRTEM and SAED analyses. To further elucidate the exceptional optical properties for the present ZnO mesocrystals, time-resolved PL measurements were conducted at room temperature. Note that time-resolved PL spectroscopy may provide quantitative information about the exciton lifetime, which represents an important indicator of the fate of charge carriers following light irradiation. Figure 4(b) compares the time-resolved PL spectra of the three ZnO structures. Evidently, ZnO mesocrystals exhibited a significantly slower PL decay than platelet and platelet/particle structures did, reflecting the essentially long-lived feature for the localized excitons in ZnO mesocrystals.

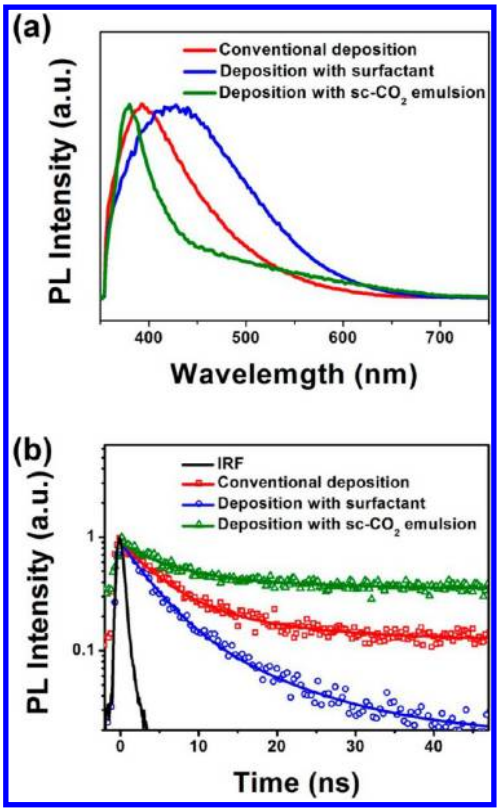

Figure 4. (a) Steady-state PL spectra and (b) time-resolved PL decays for ZnO structures prepared with different deposition conditions. In (b), the instrumental response function (IRF) and the fitting results (solid curves) were also included for comparison.

The spectra in Figure 4(b) were further fitted with a biexponential function which generates a slow (τ_1) and a fast (τ_2) decay component, respectively, assigned to radiative and nonradiative deactivation processes.[49] The intensity-average lifetime ($\langle\tau\rangle$) was then calculated to make an overall comparison of the exciton fate. As noted in Table 1, the average exciton lifetime of platelet structures, platelet/particle structures, and mesocrystals was, respectively, determined to be 7.3, 8.6, and 10.2 ns. These time constants were comparable to those recorded on high-quality ZnO tetrapods at room temperature,[50,51] in which radiative recombination was suggested to dominate the exciton decay process. It has been pointed out that the exciton dynamics of ZnO correlate tightly with several structural factors including size,[52−54] shape,[55] as well as crystallinity.[54,55] For instance, a lengthened exciton lifetime could be acquired for ZnO nanoparticles as the characteristic size increased.[54] This lifetime growth is due to the fewer surface defects existent in larger particles, which discourages the nonradiative recombination to increase the exciton decay time. On the other hand, ZnO nanostructures with different morphologies were found to exhibit different exciton dynamics, with nanorods showing the fastest exciton decay.[55] The lifetime variation originates from the nonradiative recombination centers that are correlated with the crystalline quality of the samples, in which inferior crystal quality was considered the cause for the short exciton lifetime of nanorods. As Figure 3 reveals, since the superior crystallinity of the present ZnO mesocrystals was evident, we ascribed the observed slower exciton decay to the unique mesoscopic structures of mesocrystals, i.e., the nearly single crystallinity,

dx.doi.org/10.1021/jp409607m | J. Phys. Chem. C 2013, 117, 25596−25603

which suppressed the possible nonradiative recombination processes to extend the exciton decay dynamics. The fact that ZnO mesocrystals displayed significantly depressed trap-state emission as well as reduced amplitude contribution from a fast decay component (A_2 = 35.8%) may support the above proposition.

With the highly oriented crystallinity and substantially long exciton lifetime, the present ZnO mesocrystals may find promising potentials in photoconversion applications. Particularly, the direct deposition of ZnO mesocrystals on conductive substrates facilitates their utilization as electrodes in relevant photoelectrochemical processes. To assess the applicability, we employed the as-deposited samples as the photoanode for photoelectrochemical water oxidation. Figure 5 depicts the

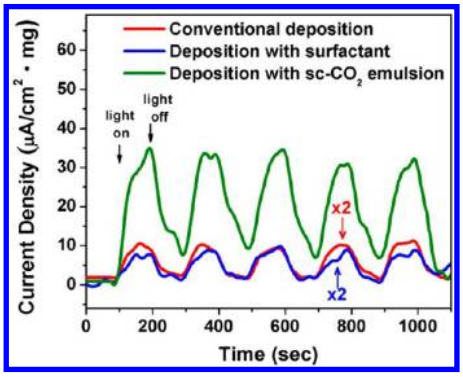

Figure 5. Chronoamperometric $I-t$ curves collected at 0 V vs Ag/AgCl for different ZnO structures under white light illumination.

chronoamperometic $I-t$ curves of the three ZnO structures recorded in 0.5 M Na_2SO_4 electrolyte under chopped light illumination. Notably, all the electrodes were prompt in generating photocurrents, suggesting the effective carrier transfer and successful electron collection for the samples during the water oxidation process. Among the three types of ZnO structures, mesocrystals achieved the largest photocurrent density of 34.4 $\mu A/cm^2$ at 0 V vs Ag/AgCl, which is about 5-fold and 8-fold higher than the value recorded on platelet (5.2 $\mu A/cm^2$) and platelet/particle structures (3.8 $\mu A/cm^2$), respectively. The superior photoelectrochemical performance of ZnO mesocrystals can be accounted for by the facile carrier transport resulting from the highly oriented crystallinity as well as the lasting exciton survival enabling the further carrier utilization. This demonstration addresses the advantage of mesocrystals and their direct deposition on conductive substrates for practical photoelectrochemical applications. It has been reported that the high crystallinity of ZnO structures may assist in suppressing the possible photocorrosion effect.[56] Since the present ZnO mesocrystals were of high crystallinity, we expected an improved photostability during their use in photoelectrochemical applications.

CONCLUSIONS

In conclusion, an effective sc-CO_2 emulsion-assisted electrochemical cathodic deposition process has been developed to prepare ZnO mesocrystals with structural features of being mesoporous and nearly single crystalline. The success of the synthetic approach relied on the introduction of sc-CO_2 emulsion in the electrolyte, which significantly increased the supersaturation degree of ZnO and improved the diffusion efficiency for NO_3^- and H_2O_2 to grow primary nanocrystals with substantially high surface energy. As a consequence of minimization of the total surface energy, preferred attachment of the primary nanocrystals along an energetically favorable orientation proceeded, eventually leading to the formation of ZnO mesocrystals. The as-deposited ZnO mesocrystals exhibited prominent excitonic band-edge emission at 380 nm with a substantially long exciton lifetime of 10.2 ns, attributable to the highly oriented crystallinity of mesocrystals that effectively suppressed the nonradiative charge recombination to extend the exciton decay dynamics. As compared to the structures prepared without the addition of surfactant or sc-CO_2, ZnO mesocrystals from sc-CO_2 emulsion showed significantly enhanced photocurrents of water oxidation, revealing their promising potential as photoanodes in relevant photoelectrochemical processes. The feasibility of the present electrochemical approach toward direct deposition of ZnO mesocrystals on conductive substrates shall foster their advanced applications in a wide array of fields, which include electrochemical cells, photovoltaic devices, as well as photoelectrochemical water splitting. The present sc-CO_2 emulsion-assisted electrochemical route can be readily extended to production of mesocrystals of other functional metal oxides, for example, TiO_2, CuO, and NiO.

AUTHOR INFORMATION

Corresponding Author

*E-mail: yhsu@cc.nctu.edu.tw. Tel.: +886-3-5712121 ext. 55317.

Notes

The authors declare no competing financial interest.

ACKNOWLEDGMENTS

This work was supported by the National Science Council of the Republic of China (Taiwan) under grants NSC-102-2113-M-009-005-MY2 and NSC-102-3113-P-009-002 and the Cabinet Office in Japan with Next Generation World-leading Researchers Program GN037.

REFERENCES

(1) Niederberger, M.; Cölfen, H. Oriented Attachment and Mesocrystals: Non-Classical Crystallization Mechanisms Based on Nanoparticle Assembly. *Phys. Chem. Chem. Phys.* **2006**, *8*, 3271−3287.
(2) Song, R.-Q.; Cölfen, H. Mesocrystals-Ordered Nanoparticle Superstructures. *Adv. Mater.* **2010**, *22*, 1301−1330.
(3) Fang, J.; Dinga, B.; Gleiter, H. Mesocrystals: Syntheses in Metals and Applications. *Chem. Soc. Rev.* **2011**, *40*, 5347−5360.
(4) Ren, Y.; Ma, Z.; Bruce, P. G. Ordered Mesoporous Metal Oxides: Synthesis and Applications. *Chem. Soc. Rev.* **2012**, *41*, 4909−4927.
(5) Geng, X.; Liu, L.; Jiang, J.; Yu, S.-H. Crystallization of $CaCO_3$ Mesocrystals and Complex Aggregates in a Mixed Solvent Media Using Polystyrene Sulfonate as a Crystal Growth Modifier. *Cryst. Growth Des.* **2010**, *10*, 3448−3453.
(6) Wang, T.; Mitchell, J.; Börner, H.; Cölfeny, H.; Antonietti, M. $BaCO_3$ Mesocrystals: New Morphologies Using Peptide−Polymer Conjugates as Crystallization Modifiers. *Phys. Chem. Chem. Phys.* **2010**, *12*, 11984−11992.
(7) Medina, D. D.; Mastai, Y. Synthesis of DL-Alanine Mesocrystals with a Hollow Morphology. *Cryst. Growth Des.* **2008**, *8*, 3646−3651.
(8) Jiang, Y.; Gong, H.; Volkmer, D.; Gower, L.; Cölfen, H. Preparation of Hierarchical Mesocrystalline DL-Lysine· HCl-Poly-(acrylic acid) Hybrid Thin Films. *Adv. Mater.* **2011**, *23*, 3548−3552.
(9) Cao, Y.; Fan, J.; Bai, L.; Hu, P.; Yang, G.; Yuan, F.; Chen, Y. Formation of Cubic Cu Mesocrystals by A Solvothermal Reaction. *CrystEngComm* **2010**, *12*, 3894−3899.

(10) Li, T.; You, H.; Xu, M.; Song, X.; Fang, J. Electrocatalytic Properties of Hollow Coral-like Platinum Mesocrystals. *ACS Appl. Mater. Interfaces* **2012**, *4*, 6942−6948.
(11) Kalyani, V.; Vasile, B. S.; Ianculescu, A.; Buscaglia, M. T.; Buscaglia, V.; Nanni, P. Hydrothermal Synthesis of $SrTiO_3$ Mesocrystals: Single Crystal to Mesocrystal Transformation Induced by Topochemical Reactions. *Cryst. Growth Des.* **2012**, *12*, 4450−4456.
(12) Jiao, W.; Wang, L.; Liu, G.; Lu, G. Q. M.; Cheng, H.-M. Hollow Anatase TiO_2 Single Crystals and Mesocrystals with Dominant {101} Facets for Improved Photocatalysis Activity and Tuned Reaction Preference. *ACS Catal.* **2012**, *2*, 1854−1859.
(13) Disch, S.; Wetterskog, E.; Hermann, R. P.; Korolkov, D.; Busch, P.; Boesecke, P.; Lyon, O.; Vainio, U.; Salazar-Alvarez, G.; Bergström, L.; Brückel, T. Structural Diversity in Iron Oxide Nanoparticle Assemblies as Directed by Particle Morphology and Orientation. *Nanoscale* **2013**, *5*, 3969−3975.
(14) Wang, M.; Zhang, Y.; Zhou, Y.; Yang, F.; Kim, E. J.; Hahn, S. H.; Seong, S. G. Rapid Room-Temperature Synthesis of Nanosheet-Assembled ZnO Mesocrystals with Excellent Photocatalytic Activity. *CrystEngComm* **2013**, *15*, 754−763.
(15) Arya, S. K.; Saha, S.; Ramirez-Vick, J. E.; Gupta, V.; Bhansali, S.; Singh, S. P. Recent Advances in ZnO Nanostructures and Thin Films for Biosensor Applications: Review. *Anal. Chim. Acta* **2012**, *737*, 1−21.
(16) Wang, Z. L.; Wu, W. Nanotechnology-Enabled Energy Harvesting for Self-Powered Micro-/Nanosystems. *Angew. Chem., Int. Ed.* **2012**, *51*, 11700−11721.
(17) Liu, Z.; Wen, X. D.; Wu, X. L.; Gao, Y. J.; Chen, H. T.; Zhu, J.; Chu, P. K. Intrinsic Dipole-Field-Driven Mesoscale Crystallization of Core-Shell ZnO Mesocrystal Microspheres. *J. Am. Chem. Soc.* **2009**, *131*, 9405−9412.
(18) Wang, S.-S.; Xu, A.-W. Template-Free Facile Solution Synthesis and Optical Properties of ZnO Mesocrystals. *CrystEngComm* **2013**, *15*, 376−381.
(19) Park, J.-H.; Choi, H.-J.; Choi, Y.-J.; Sohn, S.-H.; Park, J.-G. Ultrawide ZnO Nanosheets. *J. Mater. Chem.* **2004**, *14*, 35−36.
(20) Shi, J.; Grutzik, S.; Wang, X. Zn Cluster Drifting Effect for the Formation of ZnO 3D Nanoarchitecture. *ACS Nano* **2009**, *3*, 1594−1602.
(21) Mo, M.-S.; Lim, S. H.; Mai, Y.-W.; Zheng, R.-K.; Ringer, S. P. In Situ Self-Assembly of Thin ZnO Nanoplatelets into Hierarchical Mesocrystal Microtubules with Surface Grafting of Nanorods: A General Strategy towards Hollow Mesocrystal Structures. *Adv. Mater.* **2008**, *20*, 339−342.
(22) Zeng, Y.; Zhang, T.; Wang, L.; Wang, R. Synthesis and Ethanol Sensing Properties of Self-Assembled Monocrystalline ZnO Nanorod Bundles by Poly(ethylene glycol)-Assisted Hydrothermal Process. *J. Phys. Chem. C* **2009**, *113*, 3442−3448.
(23) Waltz, F.; Wißmann, G.; Lippke, J.; Schneider, A. M.; Schwarz, H.-C.; Feldhoff, A.; Eiden, S.; Behrens, P. Evolution of the Morphologies of Zinc Oxide Mesocrystals Under the Influence of Natural Polysaccharides. *Cryst. Growth Des.* **2012**, *12*, 3066−3075.
(24) Zeng, X.; Yuan, J.; Wang, Z.; Zhang, L. Nanosheet-Based Microspheres of Eu^{3+}-doped ZnO with Efficient Energy Transfer from ZnO to Eu^{3+} at Room Temperature. *Adv. Mater.* **2007**, *19*, 4510−4514.
(25) Wang, X.; Liu, W.; Liu, J.; Wang, F.; Kong, J.; Qiu, S.; He, C.; Luan, L. Synthesis of Nestlike ZnO Hierarchically Porous Structures and Analysis of Their Gas Sensing Properties. *ACS Appl. Mater. Interfaces* **2012**, *4*, 817−825.
(26) Li, B.; Wang, Y. Facile Synthesis and Enhanced Photocatalytic Performance of Flower-like ZnO Hierarchical Microstructures. *J. Phys. Chem. C* **2010**, *114*, 890−896.
(27) Cho, S.; Jang, J.-W.; Lee, J. S.; Lee, K.-H. Exposed Crystal Face Controlled Synthesis of 3D ZnO Superstructures. *Langmuir* **2010**, *26*, 14255−14262.
(28) Dong, J.-Y.; Lin, W.-H.; Hsu, Y.-J.; Wong, D. S.-H.; Lu, S.-Y. Ultrafast Formation of ZnO Mesocrystals with Excellent Photocatalytic Activities by a Facile Tris-Assisted Antisolvent Process. *CrystEngComm* **2011**, *13*, 6218−6222.
(29) Li, T.; Cao, Z.; You, H.; Xu, M.; Song, X.; Fang, J. Controllable Growth of ZnO Mesocrystals Using a Facile Electrochemical Approach. *Chem. Phys. Lett.* **2013**, *555*, 154−158.
(30) Tsai, W. L.; Hsu, P. C.; Hwu, Y.; Chen, C. H.; Chang, L. W.; Je, J. H.; Lin, M. H.; Groso, A.; Margaritondo, G. Building on Bubbles in Metal Electrodeposition. *Nature* **2002**, *417*, 139−139.
(31) Chang, T.-F. M.; Shimizu, T.; Ishiyama, C.; Sone, M. Effects of Pressure on Electroplating of Copper Using Supercritical Carbon Dioxide Emulsified Electrolyte. *Thin Solid Films* **2013**, *529*, 25−28.
(32) Yoshida, H.; Sone, M.; Wakabayashi, H.; Yan, H.; Abe, K.; Tao, X. T.; Mizushima, A.; Ichihara, A.; Miyata, S. New Electroplating Method of Nickel in Emulsion of Supercritical Carbon Dioxide and Electroplating Solution to Enhance Uniformity and Hardness of Plated Film. *Thin Solid Films* **2004**, *446*, 194−199.
(33) Chang, T.-F. M.; Sone, M.; Shibata, A.; Ishiyama, C.; Higo, Y. Bright Nickel Film Deposited by Supercritical Carbon Dioxide Emulsion Using Additive-Free Watts Bath. *Electrochim. Acta* **2010**, *55*, 6469−6475.
(34) Huang, C.-C.; Hsu, H.-C.; Hu, C.-C.; Chang, K.-H.; Lee, Y.-F. Morphology Control of Cathodically Deposited TiO_2 Films. *Electrochim. Acta* **2010**, *55*, 7028−7035.
(35) Hu, C.-C.; Hsu, H.-C.; Chang, K.-H. Cathodic Deposition of TiO_2: Effects of H_2O_2 and Deposition Modes. *J. Electrochem. Soc.* **2012**, *159*, D418−D424.
(36) Tena-Zaera, R.; Elias, J.; Wang, G.; Lévy-Clément, C. Role of Chloride Ions on Electrochemical Deposition of ZnO Nanowire Arrays from O_2 Reduction. *J. Phys. Chem. C* **2007**, *111*, 16706−16711.
(37) Xu, L.; Chen, Q.; Xu, D. Hierarchical ZnO Nanostructures Obtained by Electrodeposition. *J. Phys. Chem. C* **2007**, *111*, 11560−11565.
(38) Qiu, J.; Guo, M.; Wang, X. Electrodeposition of Hierarchical ZnO Nanorod-Nanosheet Structures and Their Applications in Dye-Sensitized Solar Cells. *ACS Appl. Mater. Interfaces* **2011**, *3*, 2358−2367.
(39) Zhou, L.; O'Biren, P. Mesocrystals: A New Class of Solid Materials. *Small* **2008**, *4*, 1566−1574.
(40) Xu, L.; Guo, Y.; Liao, Q.; Zhang, J.; Xu, D. Morphological Control of ZnO Nanostructures by Electrodeposition. *J. Phys. Chem. B* **2005**, *109*, 13519−13522.
(41) Degen, A.; Kosec, M. Effect of pH and Impurities on the Surface Charge of Zinc Oxide in Aqueous Solution. *J. Eur. Ceram. Soc.* **2000**, *20*, 667−673.
(42) Usui, H.; Shimizu, Y.; Sasaki, T.; Koshizaki, N. Photoluminescence of ZnO Nanoparticles Prepared by Laser Ablation in Different Surfactant Solutions. *J. Phys. Chem. B* **2005**, *109*, 120−124.
(43) Yamabi, S.; Imai, H. Growth Conditions for Wurtzite Zinc Oxide Films in Aqueous Solutions. *J. Mater. Chem.* **2002**, *12*, 3773−3778.
(44) Kawano, T.; Imai, H. Fabrication of ZnO Nanoparticles with Various Aspect Ratios through Acidic and Basic Routes. *Cryst. Growth Des.* **2006**, *6*, 1054−1056.
(45) Dong, J.-Y.; Hsu, Y.-J.; Wong, D. S.-H.; Lu, S.-Y. Growth of ZnO Nanostructures with Controllable Morphology Using a Facile Green Antisolvent Method. *J. Phys. Chem. C* **2010**, *114*, 8867−8872.
(46) Zhang, B. P.; Binh, N. T.; Wakatsuki, K.; Segawa, Y.; Yamada, Y.; Usami, N.; Kawasaki, M.; Koinuma, H. Pressure-Dependent ZnO Nanocrsytal Growth in a Chemical Vapor Deposition Process. *J. Phys. Chem. B* **2004**, *108*, 10899−10902.
(47) Kale, R. B.; Hsu, Y.-J.; Lin, Y.-F.; Lu, S.-Y. Synthesis of Stoichiometric Flowerlike ZnO Nanorods with Hundred Percent Morphological Yield. *Solid State Commun.* **2007**, *142*, 302−305.
(48) Djurišić, A. B.; Leung, Y. H. Optical Properties of ZnO Nanostructures. *Small* **2006**, *2*, 944−961.
(49) Wheeler, D. A.; Zhang, J. Z. Exciton Dynamics in Semiconductor Nanocrystals. *Adv. Mater.* **2013**, *25*, 2878−2896.
(50) Zhong, Y.; Djurišić, A. B.; Hsu, Y. F.; Wong, K. S.; Brauer, G.; Ling, C. C.; Chan, W. K. Exceptionally Long Exciton Photoluminescence Lifetime in ZnO Tetrapods. *J. Phys. Chem. C* **2008**, *112*, 16286−16295.

(51) Lee, S.-K.; Chen, S. L.; Hongxing, D.; Sun, L.; Chen, Z.; Chen, W. M.; Buyanova, I. A. Long Lifetime of Free Excitons in ZnO Tetrapod Structures. *Appl. Phys. Lett.* **2010**, *96*, 083104.
(52) Matsumoto, T.; Kato, H.; Miyamoto, K.; Sano, M.; Zhukov, E. A. Correlation between Grain Size and Optical Properties in Zinc Oxide Thin Films. *Appl. Phys. Lett.* **2002**, *81*, 1231.
(53) Hong, S.; Joo, T.; Park, W. I.; Jun, Y. H.; Yi, G.-C. Time-Resolved Photoluminescence of the Size-Controlled ZnO Nanorods. *Appl. Phys. Lett.* **2003**, *83*, 4157.
(54) Xiong, G.; Pal, U.; Serrano, J. G. Correlations among Size, Defects, and Photoluminescence in ZnO Nanoparticles. *J. Appl. Phys.* **2007**, *101*, 024317.
(55) Kwok, W. M.; Djurišić, A. B.; Leung, Y. H.; Chan, W. K.; Phillips, D. L. Time-Resolved Photoluminescence from ZnO Nanostructures. *Appl. Phys. Lett.* **2005**, *87*, 223111.
(56) Zeng, H.; Cai, W.; Liu, P.; Xu, X.; Zhou, H.; Klingshirn, C.; Kalt, H. ZnO-Based Hollow Nanoparticles by Selective Etching: Elimination and Reconstruction of MetalSemiconductor Interface, Improvement of Blue Emission and Photocatalysis. *ACS Nano* **2008**, *2*, 1661−1670.